Int. J. Heat Mass Transfer. Vol. 36, No. 8, pp. 2115–2123, 1993
Printed in Great Britain

0017-9310/93 $6.00+0.00

Binary diffusion and heat transfer in mixed convection pipe flows with film evaporation

WEI-MON YAN

Department of Mechanical Engineering, Hua Fan Institute of Technology, Shih Ting, Taipei, Taiwan 22305, R.O.C.

(*Received* 29 *April* 1992 *and in final form* 23 *September* 1992)

Abstract—A detailed numerical study has been performed to investigate the heat and mass transfer characteristics in laminar mixed convection pipe flows with film evaporation. Both the thermal conditions of constant wall temperature and uniform heat flux are considered. Results for interfacial Nusselt and Sherwood numbers are presented for air–water and air–ethanol systems for various conditions. Predicted results show that heat transfer along the gas–liquid interface is dominated by the transport of latent heat in association with the vaporization of the liquid film. Additionally, the predicted results obtained by including transport in the liquid film are contrasted with those where liquid film transport is neglected, showing that the assumption of an extremely thin film made in Lin *et al.* (*J. Heat Transfer* **110**, 337–344 (1988)) is only valid for systems with low liquid film Reynolds numbers. But for systems having a high liquid film Reynolds number Re_l, the assumption of an extremely thin film is seriously in error.

1. INTRODUCTION

INDUSTRIAL mass transfer operations are very often linked to heat transfer processes as for instance in drying, evaporation and condensation. Consequently all these processes will be influenced to some extent by coupling effects between heat and mass transfer. The interrelations can be the enthalpy flux caused by mass transfer or changes in transport properties due to variations in temperature and concentration.

In view of the complexity of the coupling between momentum, heat and mass transfer in the gas stream and momentum and heat transfer in the liquid film through their common interface, the early studies [1–5] focused on heat and mass transfer in the gas stream by assuming the liquid film to be extremely thin. Under this assumption the transport in the liquid film can be replaced by the approximate boundary conditions for the gas stream. However, their results are limited by the assumption that the liquid film on the wetted wall is negligibly thin. In practical situations, the liquid film on the wetted wall has a finite thickness, and thus the influences of the momentum and energy transport in the liquid film on the heat and mass transfer in the gas flow should be considered in the analysis.

A steady, one-dimensional model of heat and mass transfer in the evaporative cooling process that takes place in a single-tube exchanger was formulated by Perez-Blanco and Bird [6] and validated experimentally. Condor *et al.* [7] studied the vaporization of a liquid film flowing, in an order manner, down the inside surface of a tube countercurrent to a laminar gas flow. Detailed analyses, including transport processes in the flowing gas and the liquid film, were performed by Shembharkar and Pai [8] and Baumann and Thiele [9, 10] to examine the effects of a finite film thickness on the heat and mass transfer in forced convection flows. In these studies, a one-dimensional, laminar Couette flow for the liquid film was used to simplify the problem. But, because the liquid mass flow rate is high, this so-called Nusselt-type approximation for the liquid film is questionable. Recently, Yan *et al.* [11, 12] carried out an experimental and numerical study of the evaporative cooling of a laminar film falling along wetted channel walls in natural convection flows. They found that the cooling of the liquid film is mainly caused by the latent heat transfer associated with its evaporation. Often, in practical applications, the liquid film on the wetted wall is finite in thickness. This motivates the present study which examines mixed convection heat and mass transfer in a vertical tube having a wetting film of finite thickness. Hence the main objective of the present study is to extend the previous work [4] to investigate the effect of finite film evaporation on the mixed convection heat and mass transfer in a vertical pipe.

2. ANALYSIS

Partial filmwise evaporation of air–water and air–ethanol mixtures is considered in a vertical pipe with cocurrent downstream flow of both the gas stream and the falling liquid film. The thin liquid film is fed with an inlet liquid temperature T_{li} and an inlet liquid film Reynolds number Re_l. The tube wall is maintained at a constant wall temperature T_w or is heated uniformly with wall heat flux q''_w. Evaporation, heat transfer and interfacial shearing effect will lead to concentration, temperature and velocity profiles in the flow system. The interfacial heat and mass transfer is apparently determined by the coupled transport processes in the liquid film and gas flow. The transport

NOMENCLATURE

B_{in}	inlet liquid mass flow rate [kg m^{-1} s^{-1}]
c_p	specific heat [kJ kg^{-1} K^{-1}]
D	mass diffusivity [m^2 s^{-1}]
Gr_M	Grashof number (mass transfer), $g(M_a/M_v-1)(w_w-w_0)R^3/\nu_0^2$
Gr_M^*	Grashof number (mass transfer), $g(M_a/M_v-1).\overline{\dot{m}_I''}R^4/(\nu_0^2 D_0 \rho_0)$
Gr_T	Grashof number (heat transfer), $g(T_w-T_0)R^3/(\nu_0^2 T_0)$
Gr_T^*	Grashof number (heat transfer), $gq_w''R^4/(\nu_0^2 k_0)$
g	gravitational acceleration [m s^{-2}]
h_{fg}	latent heat of vaporization [J kg^{-1}]
h_M	mass transfer coefficient [m s^{-1}]
h_T	heat transfer coefficient [W m^{-2} K^{-1}]
k	thermal conductivity [W m^{-1} K^{-1}]
$\overline{\dot{m}_I''}$	average interfacial mass flux [kg m^{-2} s^{-1}]
$\dot{m}_I''$	interfacial mass flux [kg m^{-2} s^{-1}]
M_a, M_v	molar mass of air and vapor, respectively [kg mol^{-1}]
Nu_l	local Nusselt number (latent heat)
Nu_s	local Nusselt number (sensible heat)
Nu_x	interfacial Nusselt number, $Nu_s + Nu_l$
p_I	partial pressure of vapor at gas–liquid interface [kPa]
p_m	motion pressure (dynamic pressure), $p-p_0$
Pr	Prandtl number
Pr_t	turbulent Prandtl number
q_{lI}''	interfacial latent heat flux in gas side (or net enthalpy flux) [W m^{-2}]
q_{sI}''	interfacial sensible heat flux in gas side [W m^{-2}]
q_w''	heat flux at pipe wall [W m^{-2}]
r	coordinate in r-direction [m]
R	pipe radius [m]
Re_g	Reynolds number of the gas stream
Re_l	inlet liquid film Reynolds number, $4B_{in}/(2\pi R\mu_l)$
Sc	Schmidt number
Sh	interfacial Sherwood number
T	temperature [°C]
T_{li}	inlet liquid film temperature [°C]
T_w	wall temperature [°C]
u, U	dimensional and dimensionless axial velocity, respectively, $U = u/\bar{u}_0$
$\bar{u}_0$	inlet gas velocity [m s^{-1}]
u_*	shear velocity, $(\tau_w/\rho)^{1/2}$ [m s^{-1}]
v	radial velocity [m s^{-1}]
w, W	dimensional and dimensionless mass fraction of vapor, $W = (w-w_0)/(w_I-w_0)$
w_I	mass fraction of vapor at gas–liquid interface
x, X	dimensional and dimensionless axial coordinate, respectively, $X = 2x/(R\,Re_g)$
y	dimensionless wall coordinate, $(R-r)u_*/\nu$.

Greek symbols

δ	local liquid film thickness [m]
η	dimensionless radial coordinate, r/R
θ	dimensionless temperature, $(T-T_0)/(T_w-T_0)$
μ	molecular dynamic viscosity [kg m^{-1} s^{-1}]
ρ	density [kg m^{-3}]
τ_I	shear stress at the gas–liquid interface [kPa]
τ_w	wall shear stress [kPa].

Subscripts

a	of air
I	condition at the gas–liquid interface
g	of mixture (air + vapor)
l	of liquid film
o	at ambient or inlet condition
t	turbulent
v	of vapor.

processes in the liquid film are affected by the interfacial shearing effect and vaporization along the interface. While the forced gas flow is influenced by the evaporating vapor and the combined buoyancy due to thermal and solutal buoyancy forces.

2.1. *Governing equations*

(a) *Liquid film.* As mentioned above, one of the purposes of the present study is to check the suitability of the zero film thickness assumption made in previous work [4]. Hence consideration is given to a system having a sufficiently high liquid mass flow rate that the liquid film may flow turbulently. As shown in Dukler [13], the surface waves on a falling liquid film normally appear at $Re_l > 20$ except in the region near the start of the flow. The wave motion is of three-dimensional and unsteady characters. In addition, as $Re_l > 1600$, the liquid film flow would become turbulent [13]. Due to the complexity of the wave motion, an assumption of the time-wise steady film thickness which has also been used in numerous investigations [14–16] is adopted in the present study. This steady film thickness is interpreted as the temporal average of the large amplitude waves on the surface of the actual film [15]. Additionally, to facilitate the analysis, the inertial terms in the momentum equation for the liquid film are neglected [8–10], as compared with the diffusional term and gravitational term. Therefore, the two-dimensional boundary layer flow in the liquid film is governed by the following conservation equations:

axial-momentum equation

$$1/r\,.\,\partial[r(\mu_l+\mu_{lt})\partial u_l/\partial r]/\partial r+\rho_l g = 0 \quad (1)$$

energy equation

$$\rho_l c_{pl} u_l \partial T_l/\partial x = 1/r\,.\,\partial[r(k_l+k_{lt})\partial T_l/\partial r]/\partial r \quad (2)$$

where μ_{lt} and k_{lt} are the turbulent viscosity and turbulent conductivity which will be modeled in Section 3.

(b) *Gas flow*. Laminar mixed convection heat and mass transfer in the gas flow can be explored, with the usual boundary-layer approximations, by the following laminar flow equations:

continuity equation

$$\partial(r\rho_g u_g)/\partial x+\partial(r\rho_g v_g)/\partial r = 0 \quad (3)$$

axial-momentum equation

$$\rho_g u_g \partial u_g/\partial x+\rho_g v_g \partial u_g/\partial r$$
$$= -\mathrm{d}p_m/\mathrm{d}x+1/r\,.\,\partial(r\mu_g \partial u_g/\partial r)/\partial r+(\rho_g-\rho_0)g \quad (4)$$

energy equation

$$\rho_g c_{pg} u_g \partial T_g/\partial x+\rho_g c_{pg} v_g \partial T_g/\partial r = 1/r\,.\,\partial(rk_g \partial T_g/\partial r)/\partial r \quad (5)$$

concentration equation of vapor

$$\rho_g u_g \partial w/\partial x+\rho_g v_g \partial w/\partial r = 1/r\,.\,\partial(r\rho_g D\partial w/\partial r)/\partial r. \quad (6)$$

2.2. *Boundary and interfacial conditions*

The two sets of governing equations, equations (1)–(6), are subject to the following boundary conditions: at the wall the no-slip conditions for u- and v-velocities have to be satisfied as well as a constant wall temperature or uniform heat flux. On the tube axis all gradients in the mixture flow will be zero because of symmetry arguments. The inlet conditions are flat velocity, temperature and concentration distributions.

The interfacial matching conditions specified at $r = R-\delta(x)$ are described as follows:

1. continuity of velocity and temperature

$$u_I(x) = u_{g,I} = u_{l,I}, \quad T_I(x) = T_{g,I} = T_{l,I} \quad (7)$$

2. continuity of shear stress

$$\tau_I(x) = (\mu\partial u/\partial r)_{g,I} = [(\mu+\mu_t)\partial u/\partial r]_{l,I} \quad (8)$$

3. vaporizing flux of vapor into the gas flow

$$\dot{m}_I'' = \rho D/(1-w_I)\,.\,\partial w/\partial r \quad (9)$$

4. energy balance at the gas–liquid interface

$$[(k+k_t)\partial T/\partial r]_{l,I} = (k\partial T/\partial r)_{g,I}+\dot{m}_I''\,.\,h_{fg}. \quad (10)$$

At the gas–liquid interface, the liquid film equations and the gas-phase equations are coupled via boundary conditions (7)–(10). The interfacial vapor concentration and evaporating velocity can be calculated after the interfacial temperature is known [17].

$$w_I = M_v p_I/[M_a(p-p_I)+M_v p_I] \quad (11)$$

$$v_I = -D/(1-w_I)\,.\,\partial w/\partial r \quad (12)$$

where p_I is the partial pressure of the vapor at the gas–liquid interface. M_v and M_a are, respectively, the molar masses of vapor and air. By assuming that the interface is in thermodynamic equilibrium, the relation between the interfacial temperature T_I and partial pressure p_I is obtained from refs. [18, 19].

It is noted that in equation (10) the first and second terms on the right-hand side represent the interfacial sensible heat flux from the interface to the gas stream, q_{sI}'', and the net enthalpy flux to the interface due to latent heat transfer (film vaporization), q_{lI}'', respectively. The term on the left-hand side of equation (10) stands for the interfacial heat flux on the liquid side and is regarded as the total interfacial heat flux, q_I''. Therefore, the total interfacial heat flux from the interface to the gas stream can then be expressed as

$$q_I'' = q_{sI}''+q_{lI}'' = k_g \partial T_g/\partial r+\dot{m}_I''\,.\,h_{fg}. \quad (13)$$

The local Nusselt number, defined as

$$Nu_x = h_T(2R)/k_g = q_I''(2R)/[k_g\,.\,(T_I-T_b)] \quad (14)$$

can be written as

$$Nu_x = Nu_s+Nu_l \quad (15)$$

where Nu_s and Nu_l are, respectively, the local Nusselt numbers for sensible and latent heat transfer, and are defined as

$$Nu_s = (k\partial T/\partial r)_g\,.\,(2R)/[k_g\,.\,(T_I-T_b)] \quad (16)$$

and

$$Nu_l = \dot{m}_I''\,.\,h_{fg}\,.\,(2R)/[k_g\,.\,(T_I-T_b)]. \quad (17)$$

Similarly, the local Sherwood number can be found by the equation,

$$Sh = h_M\,.\,(2R)/D$$
$$= \dot{m}_I''\,.\,(1-w_I)\,.\,(2R)/[\rho_g(w_I-w_b)\,.\,D]. \quad (18)$$

Note that in the above formulation the thermophysical properties of the gas mixture and the liquid film are considered as variables depending on temperature and mixture composition. They are calculated from the pure component data by means of mixing rules [20] applicable to any multicomponent mixtures. The pure component data are approximated by polynomials in terms of temperature. The complete details on the evaluation of these properties are available in refs. [18, 19].

3. TURBULENCE MODELING

In this work, a modified Van Driest eddy viscosity model for the turbulent liquid film proposed by Yih and Liu [16] was used. The turbulent eddy viscosity is given by

$$\frac{\mu_{lt}}{\mu_l} = -0.5+0.5\{1+0.64y^2(\tau/\tau_w) \times [1-\exp(-y(\tau/\tau_w)^{1/2}/A^+)]^2 . f^2\}^{1/2} \quad \text{for } (R-r)/\delta < 0.6 \quad (19)$$

where

$$A^+ = 25.1, \quad f = \exp[-1.66(1-\tau/\tau_w)], \quad y = (R-r)u_*/\nu. \quad (20)$$

Equation (19) differs from the model used by Limberg [21] and Seban and Faghri [15] in that the shear stress and damping factor terms are modified to include the effect of interfacial shear. For $0.6 < (R-r)/\delta < 1.0$, the turbulent eddy viscosity for the liquid film is taken as constant and equal to its value at $(R-r)/\delta = 0.6$, which may be readily obtained from equation (19). The turbulent conductivity, k_{lt}, can then be obtained by introducing the turbulent Prandtl number Pr_t,

$$k_{lt} = \mu_{lt} . c_{pl}/Pr_t \quad (21)$$

where the turbulent Prandtl number can be evaluated from (Cebeci and Smith [22]):

$$Pr_t = \{1-\exp[-y(\tau/\tau_w)^{1/2}/A^+]\} / \{1-\exp[-y(\tau/\tau_w)^{1/2}/B^+]\}. \quad (22)$$

In the above equation, B^+ is available in ref. [22]. It should be mentioned here that the turbulent model used takes into account the effects of interfacial shear and wave [16]. Similar turbulent models are also used to simulate the heat transfer across a turbulent falling film by Hubbard *et al.* [14] and Seban and Faghri [15].

4. SOLUTION METHOD

The parabolic systems, equations (1)–(6) with appropriate boundary conditions, are solved by using a typical marching technique. The solution method involves a marching procedure of backward difference in axial direction, and is implicit in the radial direction. The marching procedure proceeds from the inlet to the downstream region of interest. The TDMA (Tri-Diagonal Matrix Algorithm) is employed for the solution of the resultant tri-diagonal system [23]. In the calculation the pressure can be determined by satisfying the global continuity. The iterative procedures for each axial location are ended when the relative errors in the variables, u, T, and w between two consecutive iterations are all less than 10^{-4}. To account for the change in liquid film thickness $\delta(x)$ in the flow direction due to the film vaporization and shearing effect, the interface position has to be recalculated during iteration. This in turn requires regridding during iterations with all the consequence for the computations.

During program testing, several grid sizes were employed to check the grid-independence. It is noted in the separate computations that the differences in the Nu_x from computations using either $101 \times 61 \times 31$ or $201 \times 121 \times 61$ grids are always less than 1%. Accordingly, the computations involving a $101 \times 61 \times 31$ grid are considered to be sufficiently accurate to describe the heat and mass transfer in the wetted wall system. To check further the adequacy of the computational algorithm used, the results for the limiting case of an extremely thin film under the thermal condition of constant wall temperature are first obtained. Excellent agreement between the present predictions and those of Lin *et al.* [4] was found. Another limiting case is the turbulent falling film heat transfer along a vertical plate. The predicted results agreed well with those of Yih and Liu [16]. This leads support to the employment of the present model and numerical scheme.

5. RESULTS AND DISCUSSION

In view of the large number of parameters and of the extreme demands of the computational task, a full parameteric exploration is unrealistic. Rather, the parameters were varied systematically in order to investigate the key trends in the results. In what

Table 1. Values of major parameters for various cases (constant wall temperature)

Case	T_0 °C	T_w °C	Re_l	δ_0 m	Re_g	Gr_T	Gr_M	Pr	Sc	ϕ %
				Water Film						
I	20	40	500	2.61×10^{-4}	2000	2961.95	1039.58	0.709	0.597	50
II	20	40	2000	4.53×10^{-4}	2000	2961.95	1039.58	0.709	0.597	50
III	20	40	5000	7.20×10^{-4}	2000	2961.95	1039.58	0.709	0.597	50
IV	20	60	500	2.09×10^{-4}	2000	5923.89	3300.03	0.709	0.597	50
V	20	60	2000	3.62×10^{-4}	2000	5923.89	3300.03	0.709	0.597	50
VI	20	60	5000	5.74×10^{-4}	2000	5923.89	3300.03	0.709	0.597	50
				Ethanol Film						
VII	20	40	500	3.51×10^{-4}	2000	2936.51	−4061.50	0.710	1.312	0
VIII	20	40	2000	6.12×10^{-4}	2000	2936.51	−4061.50	0.710	1.312	0
IX	20	40	5000	9.80×10^{-4}	2000	2936.51	−4061.50	0.710	1.312	0
X	20	60	500	2.86×10^{-4}	2000	5873.03	−9237.44	0.710	1.312	0
XI	20	60	2000	4.97×10^{-4}	2000	5873.03	−9237.44	0.710	1.312	0
XII	20	60	5000	7.92×10^{-4}	2000	5873.03	−9237.44	0.710	1.312	0

Table 2. Values of major parameters for various cases (uniform wall heat flux)

Case	T_0 °C	q''_w $W\,m^{-2}$	Re_l	Re_g	Gr^*_T	Gr^*_M	Pr	Sc	ϕ %
					Water Film				
I	20	2500	500	2000	143 604.5	502.15	0.709	0.597	50
II	20	2500	2000	2000	143 604.5	270.95	0.709	0.597	50
III	20	2500	5000	2000	143 604.5	233.81	0.709	0.597	50
IV	20	5000	2000	2000	287 208.9	350.99	0.709	0.597	50
V	20	10 000	2000	2000	574 417.8	549.0	0.709	0.597	50

follows, results are particularly presented for water and ethanol film evaporations. Various cases shown in Tables 1 and 2 were selected to examine the effects of liquid film evaporation on mixed convection heat and mass transfer in a vertical tube. In Tables 1 and 2, the relative humidity of the ambient air ϕ is assigned as 50% for air–water mixture and 0% for air–ethanol vapor mixture which are often encountered in practice. It is also noted that the inlet liquid film Reynolds number and the corresponding inlet film thickness are listed in Table 1. All of the cases are based on a vertical tube of radius $R = 0.01$ m.

(A) *Constant wall temperature*

To check the suitability of the assumption of zero film thickness made in Lin *et al.* [4], the axial velocities predicted with finite and zero film thicknesses are contrasted in Fig. 1. It is clear that the difference in the shape of the velocity profiles between these two treatments (i.e. considering a finite film thickness and neglecting film thickness) is substantial. The gas velocity in the core remains relatively uniform for the results of finite film thickness. This is clearly due to the shearing effect created by the falling liquid film. For the results of zero film thickness, the velocity profiles develop from the uniform distributions at the inlet to the parabolic ones in the downstream region. But, the gas mass flow rate keeps increasing due to the evaporation of water vapor into the gas stream from the liquid film. It is also noticed that a rise in T_w would result in a higher axial velocity U, in conformity with a greater amount of water vapor evaporating into the gas stream for a higher T_w.

Shown in Figs. 2(a) and (b) are the axial developments of temperature and concentration profiles, respectively. An overall inspection of Figs. 2(a) and (b) reveals that both θ and W develop in a very similar fashion. Careful inspection, however, discloses that the mass-fraction boundary layers develop a little more rapidly than the temperature boundary layers do. This is due to the fact that the Prandtl number Pr is slightly larger than the Schmidt number Sc. It is noteworthy that a higher mass-fraction of water vapor is found at the downstream of the tube for case III compared to case II. This is the direct consequence of a larger amount of water vapor evaporating into the gas stream for systems having a higher liquid film Reynolds number Re_l. This confirms the general concept that for a falling film heat transfer, the interfacial heat and mass transfer is more profound for a system having a higher Re_l [15, 16].

To study the relative contributions of heat transfer

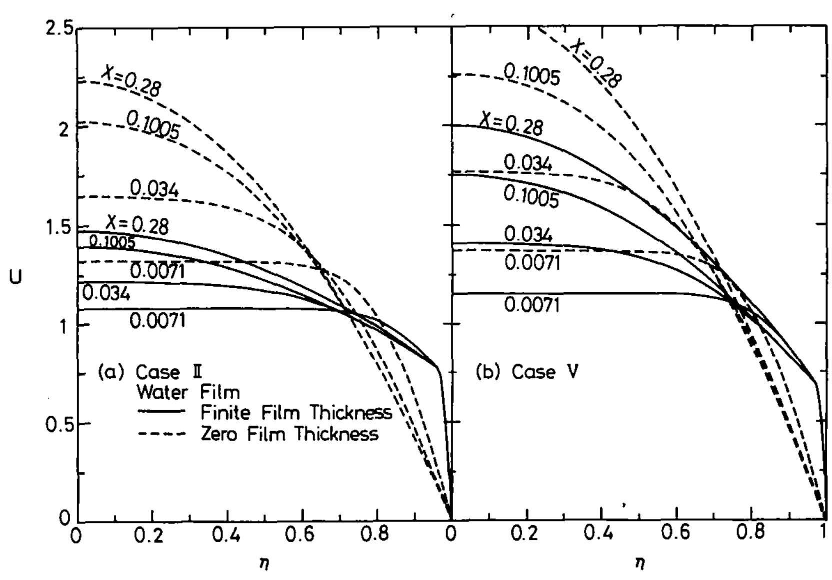

FIG. 1. Developments of axial velocity profiles.

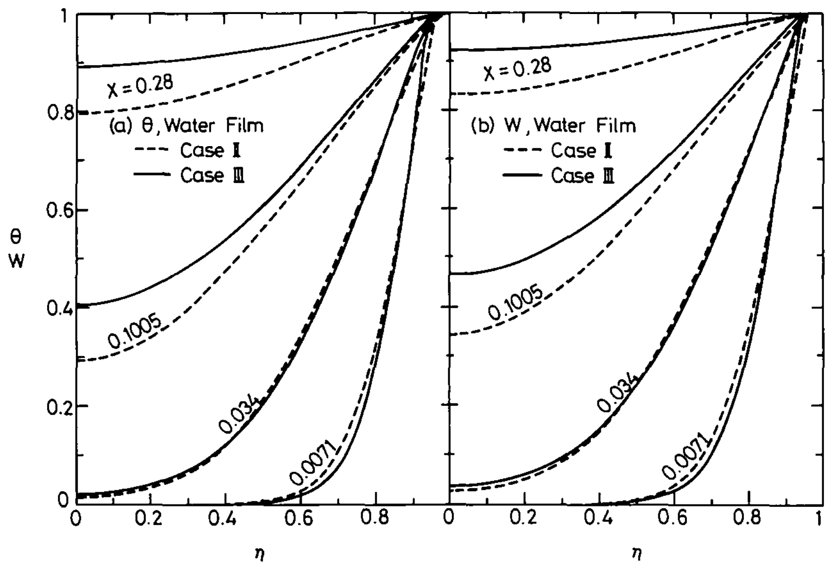

FIG. 2. Developments of axial temperature and mass-fraction profiles.

through sensible and latent heat exchanges across the gas–liquid interface, three kinds of Nusselt numbers are presented in Fig. 3. According to the results in Fig. 3(a), systems with a higher Re_l show a larger interfacial sensible heat Nusselt number Nu_s (by comparing cases II and III). Moreover, a smaller Nu_s results for a higher T_w (by comparing cases II and V). This is due to the larger evaporating (blowing) and

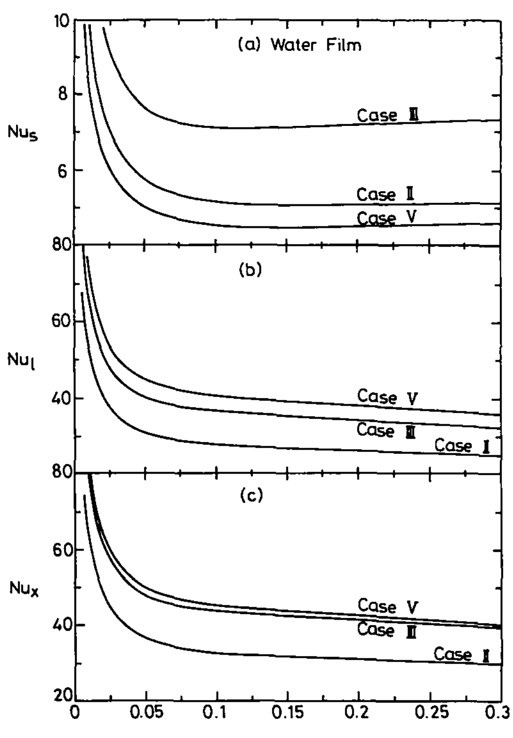

FIG. 3. Axial distributions of local Nusselt numbers. (a) Sensible heat Nusselt number; (b) Latent heat Nusselt number; (c) Interfacial Nusselt number.

opposing buoyancy effects for systems having a higher T_w. In Fig. 3(b) the system with a higher wall temperature shows higher values for Nu_l (cases II and V). This is brought about by the larger latent heat transport associated with the greater film evaporation for a higher T_w. Comparing the ordinate scales of Figs. 3(a) and (b) indicates that the magnitude of Nu_l is much larger than that of Nu_s implying that the heat transfer resulting from latent heat exchange is much more effective. Also clearly seen in Fig. 3(b) is the effects of the Re_l on the distributions of Nu_l. The higher the liquid film Reynolds number Re_l the larger is Nu_l. In Fig. 3(c), Nu_x, the sum of Nu_s and Nu_l is presented.

Comparisons are made in Figs. 4 and 5 to check the suitability of the assumption of zero film thickness by examining the distributions of interfacial Nusselt number Nu_x and Sherwood number Sh predicted in the presence and absence of a finite liquid film. It is clearly seen that the magnitudes of Nu_x and Sh are underpredicted in the case where a negligible film thickness is assumed. Moreover, the difference between these two treatments increases with the liquid film Reynolds number Re_l. This implies that the assumption of an extremely thin film is a limiting case and is valid only for systems having a small liquid flow rate. For high liquid film Reynolds numbers, the assumption of zero film thickness can produce considerable error. By comparing the corresponding curves in Figs. 5(a) and (b), it is found that a larger Sh results for systems with a lower T_w. In addition, a larger Sh is experienced for a higher Re_l.

After examining the mixed convection heat and mass transfer with water film evaporation in a vertical tube, attention is turned to the effects of ethanol film evaporation on this process. The axial distributions of interfacial Nusselt number Nu_x and Sherwood number Sh for ethanol film evaporation in Figs. 6 and 7

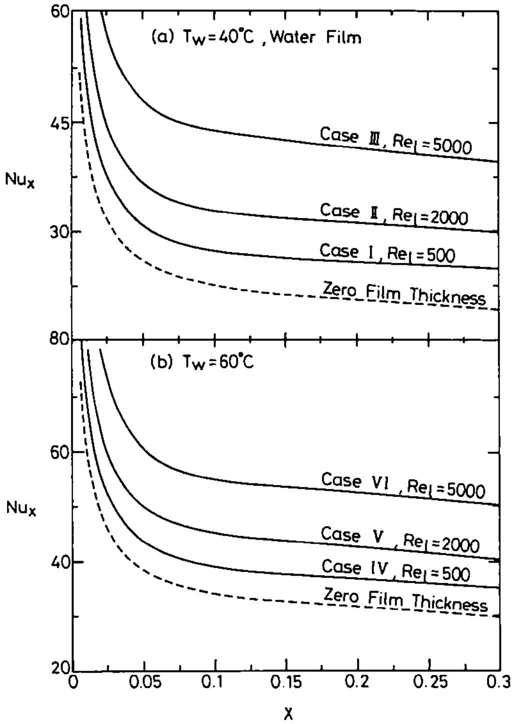

FIG. 4. Axial distributions of interfacial Nusselt number Nu_x.

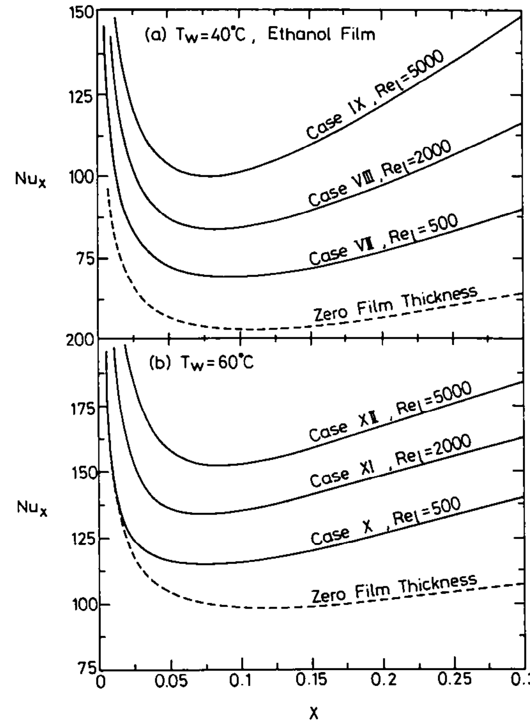

FIG. 6. Axial distributions of interfacial Nusselt number Nu_x for ethanol film evaporation.

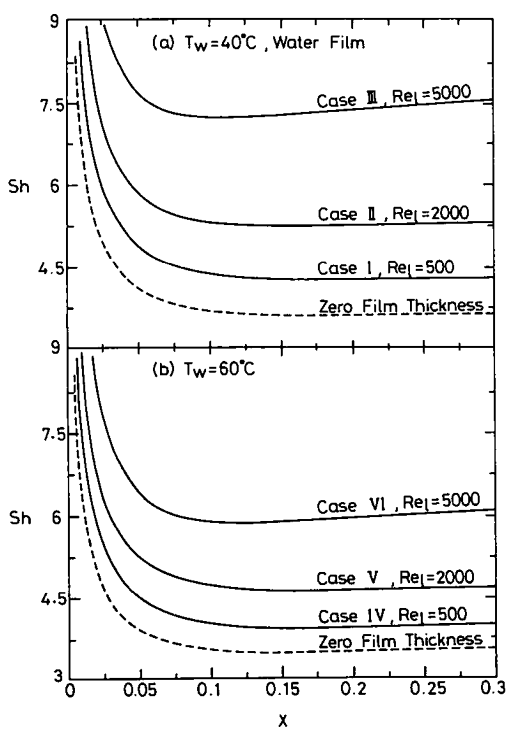

FIG. 5. Axial distribution of local Sherwood number Sh.

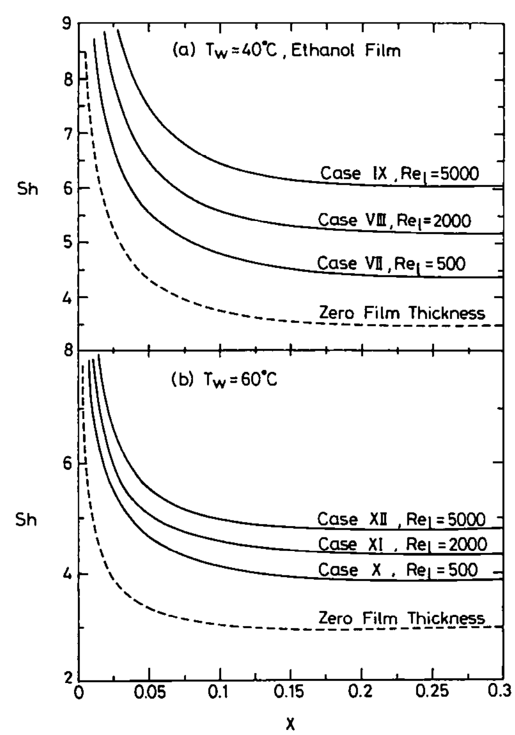

FIG. 7. Axial distributions of local Sherwood number Sh for ethanol evaporation.

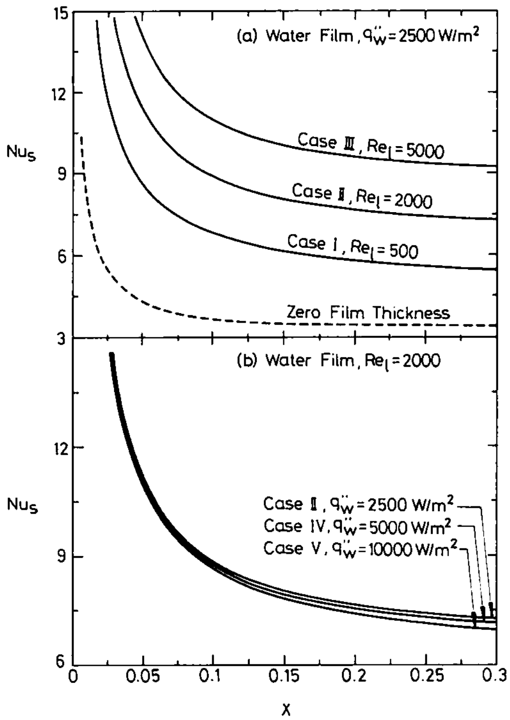

FIG. 8. Axial distributions of local sensible heat Nusselt number Nu_s.

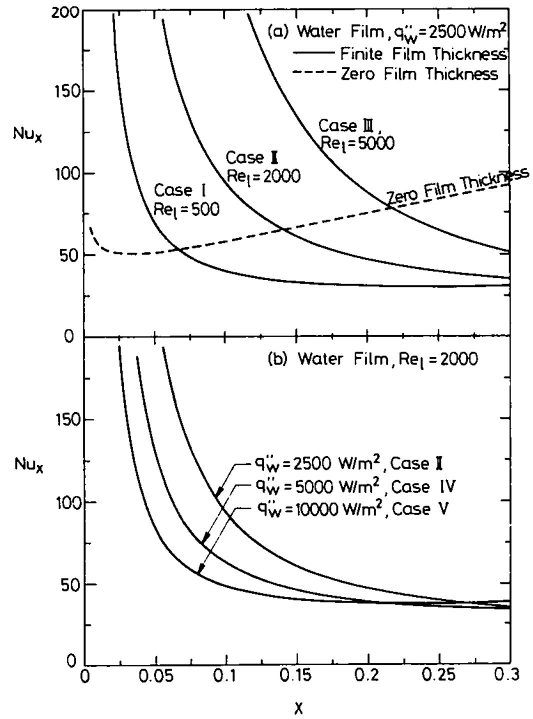

FIG. 9. Axial distributions of interfacial Nusselt number Nu_x.

are the counterpart of those in Figs. 4 and 5. As in the case of water film evaporation, the results of zero film thickness underpredict the local Nu_x and Sh. Moreover, the deviations in Nu_x and Sh between these two treatments become significant as Re_l increases. Comparing Figs. 4 and 6 shows that the magnitude of Nu_x is larger for ethanol film evaporation. This implies that the mixed convection heat exchange associated with ethanol film evaporation is much more effective than that with water film evaporation under the same thermal conditions.

(B) *Uniform heat flux*

In this section solutions for uniform heat flux boundary conditions are presented. The effects of liquid film Reynolds number Re_l on the local sensible heat Nusselt number Nu_s under the thermal condition of uniform heat flux are shown in Fig. 8(a). For comparison purposes, the results of zero film thickness are plotted together in this plot. It is clearly found that the difference between those two approaches increases with Re_l. It is concluded that the assumption of an extremely thin thickness is always inappropriate in both the thermal conditions of constant wall temperature and uniform heat flux, especially for high Re_l. Figure 8(b) shows the effects of wall heat flux q''_w on the Nu_s. A slightly smaller Nu_s is noted for a higher q''_w due to the larger evaporating (blowing) effects for a higher q''_w.

Figure 9 gives the influences of Re_l and q''_w on the distributions of interfacial Nusselt number Nu_x. Like the results of constant wall temperature, a larger Nu_x results for systems having a higher Re_l. In Fig. 9(a), near the entrance the results of zero film thickness underpredict the Nu_x. But as the flow goes downstream, the results of zero film thickness overpredict the Nu_x. Results are also found in Fig. 9(b)

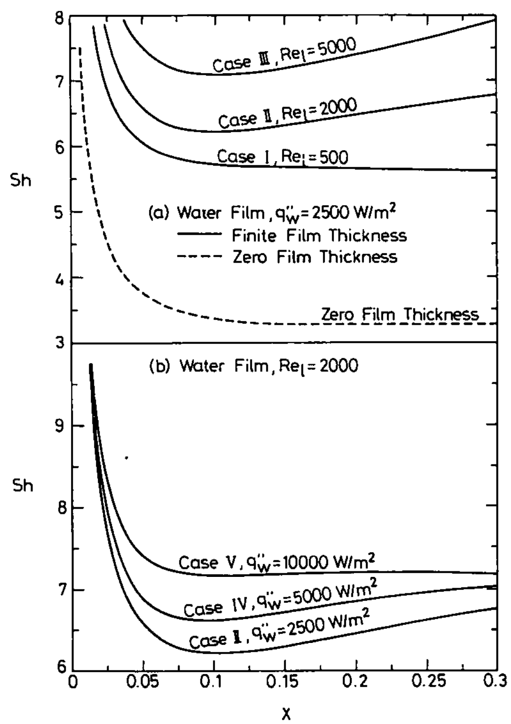

FIG. 10. Axial distributions of local Sherwood number Sh.

for the effect of q''_w on the Nu_x distributions—for $X < 0.2$, the Nu_x is larger for a smaller q''_w.

The distributions of the interfacial Sherwood number Sh are depicted in Fig. 10 for various Re_l and q''_w to illustrate the mass transfer characteristics. Similar to the results given in Fig. 10(a) for Nu_x, a larger Sh is found for a higher Re_l. In addition, the results of zero film thickness underpredict the Sh. The results in Fig. 10(b) indicate that a larger Sh is noted for systems with a larger q''_w. This outcome apparently results from the larger interfacial evaporating rate for a higher q''_w, which in turn results in a larger Sh.

6. CONCLUSIONS

A numerical study has been carried out to explore the effects of film evaporation on mixed convection heat and mass transfer by solving the governing equations for the gas stream and liquid film coupled through interfacial matching conditions. The influences of the thermal conditions and the inlet liquid film Reynolds number on the momentum, heat and mass transfer in the flow are investigated in detail. In particular, comparative results are presented for both water and ethanol film evaporations to check the suitability of the assumption of zero film thickness. The major results are briefly summarized as follows:

(1) Heat transfer between the interface and gas stream is dominated by the transport of latent heat in conjunction with the film vaporization.

(2) A smaller Nu_x is experienced for systems with a higher T_w (or q''_w). This is due to the larger evaporating (blowing) effect along the gas–liquid interface for a higher T_w (or q''_w).

(3) Larger Nusselt numbers and Sherwood numbers result for a higher Re_l due to the larger shearing effects created by the falling film.

(4) The assumption of an extremely thin film thickness is a limiting condition and is only valid for systems with a relatively low liquid mass flow rate. But for high liquid film Reynolds numbers Re_l the assumption would cause serious errors.

Acknowledgement—The financial support of this work by the National Science Council, R.O.C., through the contract NSC81-0401-E211-502 is greatly appreciated.

REFERENCES

1. L. C. Chow and J. N. Chung, Evaporation of water into a laminar stream of air and superheated steam, *Int. J. Heat Mass Transfer* **26**, 373–380 (1983).
2. J. Schroppel and F. Thiele, On the calculation of momentum, heat and mass transfer in laminar and turbulent boundary layer flows along a vaporizing liquid film, *Numer. Heat Transfer* **6**, 475–496 (1983).
3. C. H. Wu, D. C. David, J. N. Chung and L. C. Chow, Simulation of wedge-shaped product dehydration using mixtures of superheated steam and air in laminar flow, *Numer. Heat Transfer* **11**, 109–123 (1987).
4. T. F. Lin, C. J. Chang and W. M. Yan, Analysis of combined buoyancy effects of thermal and mass diffusion on laminar forced convection heat transfer in vertical tube, *J. Heat Transfer* **110**, 337–344 (1988).
5. W. M. Yan and T. F. Lin, Natural convection heat transfer enhancement through latent heat transport in vertical parallel plate channel flows, *Can. J. Chem. Engng* **68**, 360–367 (1990).
6. H. Perez-Blanco and W. A. Bird, Study of heat and mass transfer in vertical-tube evaporative cooler, *J. Heat Transfer* **106**, 210–215 (1984).
7. J. R. Condor, D. J. Gunn and M. A. Shaikh, Heat and mass transfer in two-phase flow—a mathematical model for laminar film flow and its experimental validation, *Int. J. Heat Mass Transfer* **25**, 1113–1126 (1982).
8. T. R. Shembharkar and B. R. Pai, Prediction of film cooling with a liquid coolant, *Int. J. Heat Mass Transfer* **29**, 899–908 (1986).
9. W. W. Baumann and F. Thiele, Heat and mass transfer in two-component film evaporation in a vertical tube, *Proc. 8th Int. Heat Transfer Conf.* **5**, 1843–1848 (1986).
10. W. W. Baumann and F. Thiele, Heat and mass transfer in evaporating two-component liquid film flow, *Int. J. Heat Mass Transfer* **33**, 267–273 (1990).
11. W. M. Yan, T. F. Lin and Y. L. Tsay, Evaporative cooling of liquid film through interfacial heat and mass transfer in a vertical channel—I. Experimental study, *Int. J. Heat Mass Transfer* **34**, 1105–1111 (1991).
12. W. M. Yan and T. F. Lin, Evaporative cooling of liquid film through interfacial heat and mass transfer in a vertical channel—II. Numerical study, *Int. J. Heat Mass Transfer* **34**, 1113–1124 (1991).
13. A. E. Dukler, Characterization, effects and modeling of the wavy gas–liquid interface, *Prog. Heat Mass Transfer* **6**, 207–234 (1972).
14. G. L. Hubbard, A. F. Mills and D. K. Chung, Heat transfer across a turbulent falling film with cocurrent vapor flow, *J. Heat Transfer* **98**, 319–320 (1976).
15. R. A. Seban and A. Faghri, Evaporation and heating with turbulent falling liquid films, *J. Heat Transfer* **98**, 315–318 (1976).
16. S. M. Yih and J. L. Liu, Prediction of heat transfer in turbulent falling liquid films with or without interfacial shear, *A.I.Ch.E. Jl* **29**, 903–909 (1983).
17. E. R. G. Eckert and R. M. Drake, Jr., *Analysis of Heat and Mass Transfer*, Chapters 20 and 22. McGraw-Hill, New York (1972).
18. T. Fujii, Y. Kato and K. Mihara, Expressions of transport and thermodynamic properties of air, steam and water, Sei San Ga Ken Kyu Jo, Report No. 66, Kyu Shu Dai Gaku, Kyu Shu, Japan (1977).
19. JSME Data, Thermophysical Properties of Fluids, The Japan Society of Mechanical Engineers (1983).
20. R. B. Bird, W. E. Stewart and E. N. Lightfood, *Transport Phenomena*. Wiley, New York (1960).
21. H. Limberg, Warmeubergang an turbulente und laminare rieselfilme, *Int. J. Heat Mass Transfer* **16**, 1691–1698 (1973).
22. T. Cebeci and A. M. O. Smith, *Analysis of Turbulent Boundary Layers*. Academic Press, New York (1974).
23. S. V. Patankar, *Numerical Heat Transfer and Fluid Flow*, Chapter 6. Hemisphere/McGraw-Hill, New York (1980).